A EUROPEAN JOURNAL

CHEMPHYSCHEM

OF CHEMICAL PHYSICS AND PHYSICAL CHEMISTRY

Accepted Article

Title: Interfacial Study of Nickel Modified Pt(111) Surfaces in Phosphate Containing Solutions. Effect on the Hydrogen Evolution Reaction

Authors: Juan M. Feliu, Francisco J. Sarabia, and Víctor Climent

To be cited as: *ChemPhysChem* 10.1002/cphc.201900543

Link to VoR: http://dx.doi.org/10.1002/cphc.201900543

A Journal of

ChemPubSoc Europe

WILEY-VCH

www.chemphyschem.org

Interfacial Study of Nickel Modified Pt(111) Surfaces in Phosphate Containing Solutions. Effect on the Hydrogen Evolution Reaction.

Francisco J. Sarabia, Víctor Climent, and Juan M. Feliu*

Instituto Universitario de Electroquímica, Universidad de Alicante, Carretera San Vicente del Raspeig s/n, E-03690 San Vicente del Raspeig, Alicante, Spain

Abstract

The surface modification of electrodes presents great interest in electrocatalysis. Deposition of foreign adatoms on the surface of the electrode can originate a significant enhancement in the catalytic activity. It has been reported that nickel deposits on Pt surfaces improve the rate of the hydrogen evolution reaction (HER, *Nature Energy* 2017, 2, 17031). During the deposition process of such metal adlayers, the pH and the nature of the ions in the electrolyte play an important role. Phosphate species are typically used to prepare buffer solutions in a wide range of pH. However, the effect of phosphate on platinum surface modification with nickel deposits has not been studied yet. In this work, new data about the interaction of phosphate with nickel adatoms deposited on Pt(111) at pH 5 is investigated using cyclic voltammetry and infrared spectroscopy. The results show that, when nickel is in solution, the phosphate ions are adsorbed at lower potentials than in the absence of nickel. Laser-Induced Temperature Jump Technique demonstrates that nickel facilitates the adsorption of phosphate because of a shift of the pzc toward negative potentials. This increases the magnitude of the positive electric field on the electrode surface, at a given potential E>pzc, facilitating the adsorption of anions. CO displacement technique has been also employed to obtain additional information about co-adsorbed phosphate on nickel adlayers. Finally, the HER has been studied at pH 5 in the presence of nickel, with and without phosphate in the bulk solution.

Keywords: platinum single crystal; nickel underpotential deposition; hydrogen evolution reaction; potential of zero charge; phosphate adsorption

1. Introduction

There is great interest in the study of different methodologies for the surface modification of electrodes. It has been demonstrated in many occasions that the deposit of foreign atoms on particular substrates can improve the catalytic activity of certain electrochemical reactions. In some cases, this improvement is due to a modification of the electronic properties of the substrate caused by a displacement of the d-band in the density of states of the metal towards the fermi level [1]. In other cases, the adatoms produce a bifunctional effect, resulting in the creation of new active sites. In particular, it has been found that Ni and Sn are very good catalysts for the oxidation of CO, since their oxophilic nature facilitates the adsorption of oxygenated species that are necessary for this reaction [2]. Another mechanism by which adatoms can improve a reaction is the third body effect. In this case, specific sites on the substrate are blocked to prevent parallel pathways that are detrimental to the desired reaction [3].

Single crystal surfaces provide well defined substrates that allow the study of the effects described above under highly controlled conditions. They allow, in many cases, to obtain a regular and controlled distribution of adatoms and, therefore, to know, with high accuracy, the main geometric properties of the deposits being formed on the single crystal surface. At the same time, this also allows to obtain additional information about the effect of the geometry of the active sites, where the adsorption of intermediates takes place, since this affects the activation energy and the reaction rate. The deposition of some adatoms is produced at a higher potential than the Nernstian potential for the bulk deposition [4]. This phenomenon is known as underpotential deposition (upd). In this case, the amount of adsorbed adatoms on the substrate surface, the coverage, is closely linked to the potential applied to the electrode.

The stability of such adatom deposits is critical for their application in electrocatalysis. In this regard, the solution pH is a key parameter affecting the stability of most adatoms. In previous studies, nickel deposits were characterized on Pt (111) at pH close to 5 and at pH 13. In addition, the effect of the different nickel coverages on Pt (111) in the oxidation of CO at pH 13 and 4.5, and in the hydrogen evolution reaction at pH 13 was

studied. It was observed that nickel on Pt (111) improves the catalytic activity for both reactions [5].

Another factor that plays an important role in the formation of metal adlayers is the nature of the anions present in the solution. The anions, on the one hand, can compete with the adatoms for the adsorption sites on the surface of the substrate. On the other hand, anions can be adsorbed on top of the deposited upd adlayer thus interfering in the catalysis of electrochemical reactions [6]. In this regard, while typical solutions close to the neutral pH involve the use of phosphate buffer, the competitive interaction of phosphate species with nickel deposits on platinum has not been studied yet.

The use of phosphate buffer solutions allows to control the pH in a wide range. In addition, phosphate species are electrolytes used in a large number of applications such as fuel cells or biosensors [7]. In this work we study the interaction of phosphate ions with the surface of Pt (111) modified with nickel at pH 5, and the effect that it causes on the reaction of hydrogen evolution.

2. Experimental

2.1 Electrochemical Experiments

Working electrodes were prepared from small beads, ca. 2 mm in diameter, obtained by the method described by Clavilier et al. [8]. Prior to each experiment, the working electrodes were flame annealed in a propane-oxygen flame, cooled down in a hydrogen/argon (1:3) atmosphere and transferred to the cell protected by a drop of ultra-pure water saturated with these gases [8b].

The experiments were performed at room temperature in a classical three electrode cell configuration using a Luggin capillary to separate the reference electrode from the main working solution. A coiled platinum wire was used as counter electrode. A Ag/AgCl/KCl saturated electrode was used as reference for FTIRRAS. A Pd-H_2 electrode was used as reference for the laser temperature jump technique, and a reversible hydrogen electrode (RHE) was used as reference for the rest of the electrochemical experiments. The Luggin capillary was filled with the same solution as

the main compartment of the cell. The working electrode was contacted with the solution in the hanging meniscus configuration. Potential control was attained with a potentiostat (eDAQ EA161) connected with a signal generator (PAR 173) and a digital recorder (eDAQ, ED401). HER experiments were carried out using a ED101 rotating disk electrode and a CTV 101 rotation rate controller (Radiometer Analytical).

2.2 Chemicals

Solutions were prepared using disodium monohydrogen phosphate (Merck Suprapur), sodium fluoride (Merck Suprapur), perchloric acid (Merck Suprapur) and ultrapure water from Elga Purelab Ultra Analytic system (Resistivity 18.2 MΩ cm). Nickel sulfate (Sigma-Aldrich 99.99%) was also used to add nickel (II) to the solution. Argon, hydrogen and CO (N50, Air liquid) were used for deaerating the solution, to cool down the electrode after the flame annealing and for the CO displacement experiments, respectively. Solutions were deaerated by bubbling Ar for at least 15 min before starting each experiment. During the experiments, an Ar blanket was maintained above the solution to prevent the entrance of O_2 into the cell. The pH of the solutions was measured using a pH-basic-20 pH-meter from Crison coupled with a pH-probe pH 50 12 HACH model.

2.3 CO Displacement Technique

CO displacement experiments were performed by following the same methodology as previously reported [9]. The experiments consist on the following steps: I) After recording the voltammogram, potential cycling was stopped at 0.1 V (in this work, the polarization time at 0.1V before the start of the displacement experiment is very important because it determines the amount of adsorbed nickel on the surface of the electrode [5b], and therefore it was carefully controlled). II) A flow of CO was introduced into the electrochemical cell while the transient current, produced in response to the introduction of this gas, was recorded. It is very important to avoid the entrance of O_2 into the experimental system by flushing permanently either Ar or CO. III) When the current decays to zero, indicating saturation of the surface, the CO flow was stopped, and Ar was bubbled (during 15 min) into the solution to remove the excess

of CO dissolved in solution. IV) Next, the surface blockage was checked in the low potential range and finally, the CO adsorbed on the surface was stripped to recover the initial stable voltammetric profile.

2.4 Fourier Transform Infrared-Reflection Absorption Spectroscopy

In situ external reflection infrared experiments were carried out with a Nicolet 8700 (Thermo Scientific) spectrometer equipped with an MCT-A detector using p-polarized light and with a spectral resolution of 8 cm^{-1}. The glass spectroelectrochemical cell was equipped with a prismatic BaF_2 window beveled at 60°. This window allows extending the spectroscopic window below 1000 cm^{-1} allowing identification of phosphate bands [10]. A Ag/AgCl/KCl saturated electrode in a separate compartment was used as reference in this case, but all potentials have been converted to the RHE scale. The Pt(111) working electrode used in these experiments was ca. 4.5 mm in diameter and was prepared and treated before experiments in a similar way as the smaller samples used in the voltammetric experiments. The spectra are plotted in absorbance units ($-\log(R/R_0)$) by referring the single beam reflectance spectrum collected at the sample potential (R) to the one collected at the reference potential (R_0). The reference potential was selected as 0.1 V for the study of the phosphate bands. The methodology of this experiment consists of the following steps: I) The working electrode was introduced at 0.1 V in the solution containing 0.2M Na_2HPO_4/ $HClO_4$ (pH=5) plus 0.1M NaF/ $HClO_4$ (pH=5), and was pressed against the BaF_2 window, holding at all times the electrode potential at the initial value. II) Then, after recording the initial spectrum, the potential was sequentially stepped to increasing values and spectra were recorded at each potential until 0.95V. III) The next step was to introduce 1mM $NiSO_4$ $6H_2O$ dissolved in 0.2M Na_2HPO_4/ $HClO_4$ plus 0.1M NaF/ $HClO_4$ (pH=5) into the cell and to repeat the same steps above, after flame annealing of the electrode. 200 interferograms were collected at each potential.

2.5 Laser-Induced Temperature Jump Technique

The procedure for recording the laser induced transients was described in detail elsewhere [11]. Before recording the laser transient, several voltammetric cycles were

recorded to ensure the cleanliness and stability of the system. A second auxiliary electrode is used as an internal reference to measure the potential transient. At the beginning, both working and the second auxiliary electrode are polarized at the same potential and 200 μs before firing the laser both electrodes are disconnected from the potentiostat. The potential transients record the change in the potential of the working electrode with respect to the second auxiliary electrode under coulostatic conditions (open circuit). Each experiment is repeated with a frequency of 10Hz to ensure that the temperature relaxes to the initial value between measurements. Either 128 or 256 potential transients are recorded and averaged using a Tektronix Model TDS 3054B oscilloscope.

The duration of the pulse is 5ns and the laser used is a 532 nm frequency (double harmonic) Nd-YAG (Brilliant B from Quantel). A standard arrangement of lenses is used to reduce the diameter of the laser beam from 6 mm to 4 mm. The energy density of the laser beam is reduced to less than 8mJ/cm^2 by combining the effect of an attenuator from Newport Corporation (Model M-935-10) and the regulation of the Q-switch time. The laser energy was measured with a piroelectric sensor head (Model M-935-10).

3. Results and discussion

3.1 Cyclic Voltammograms

Figure 1 shows the cyclic voltammograms of a Pt(111) surface in 1 mM nickel sulphate solution at pH 5 with (red curve) and without phosphates (black curve). The blank voltammogram obtained without nickel in 0.1M $Na_2HPO_4/HClO_4$ is also included for the sake of comparison (green curve). In agreement with previous reports, the voltammogram obtained in the presence of Ni without phosphate show peaks in the hydrogen adsorption/desorption region at 0.3 V (negative scan, peak a'1) and 0.4 V (positive scan, peak a1). Those peaks correspond to the coadsorption and desorption of the Ni hydroxyl, respectively [5b]. The blank voltammogram recorded in solution containing phosphate (green curve in figure 1) shows the well-known adsorption-desorption processes of phosphate at potentials above 0.4 V for positive and negative sweep respectively, with an average charge of 113 μC/cm^2. This charge might also include some amount of OH coadsorption. The integrated charge involved in the hydrogen reductive adsorption (negative scan) and oxidative desorption (positive scan)

zone (0.06-0.4 V) amounts to 138 μC/cm^2 in this case. This value is slightly lower than the corresponding charge recorded in pH =1, in accordance with previous reports [12]. When both nickel and phosphate ions are in the solution (red curve), the nickel desorption peak, previously at 0.4 V, is shifted and overlapped with the adsorption of phosphate, resulting in a single peak at 0.67 V (peak b1) in the positive-going scan with a charge of 205 μC/cm^2. On the one hand, for the negative-going scan, the reductive desorption of phosphate ions occurs above 0.4 V (peak b'1), in a peak that resembles the one recorded in the absence of nickel. Besides, in the zone of hydrogen adsorption, a peak appears at 0.35 V (peak b''1) corresponding to the Ni^{2+} deposition. This peak potential is also positively shifted in comparison with the one recorded without phosphate (peak a'1). The integrated charge involved in those two processes (peaks b'1 and b''1, from 0.85 to 0.25V) in the negative-going scan (205μC/cm^2) equal in absolute value the one obtained for the peak in the positive sweep (peak b1). Comparing the cyclic voltammograms for Pt(111) surface in 1 mM $NiSO_4$ with and without phosphate ions, it is clear that the effect of phosphate to the nickel adsorption-desorption processes is an overall shift to higher potentials. In addition, the difference between the corresponding peak potentials for these processes increases, evidencing an increasing irreversibility in nickel adsorption-desorption due to the presence of phosphate ions in the solution. This fact might suggest that phosphate induces the nickel adsorption on the Pt(111) surface, most likely in a coadsorption process, resulting in a more stable nickel deposit than when there are not phosphate ions in the solution. It is worth noting that previous reports have demonstrated that nickel hydroxide adsorbed on the Pt(111) surface shifts the pzc to lower potential[5a, 5c]. Therefore, for a given potential, the surface would carry more charge when nickel is present. This increase of positive charge could facilitate the anion adsorption on the nickel adlayer at lower potentials. Therefore, a synergic effect between phosphate and nickel adsorption might be at the core of the observed trends.

10.1002/cphc.201900543

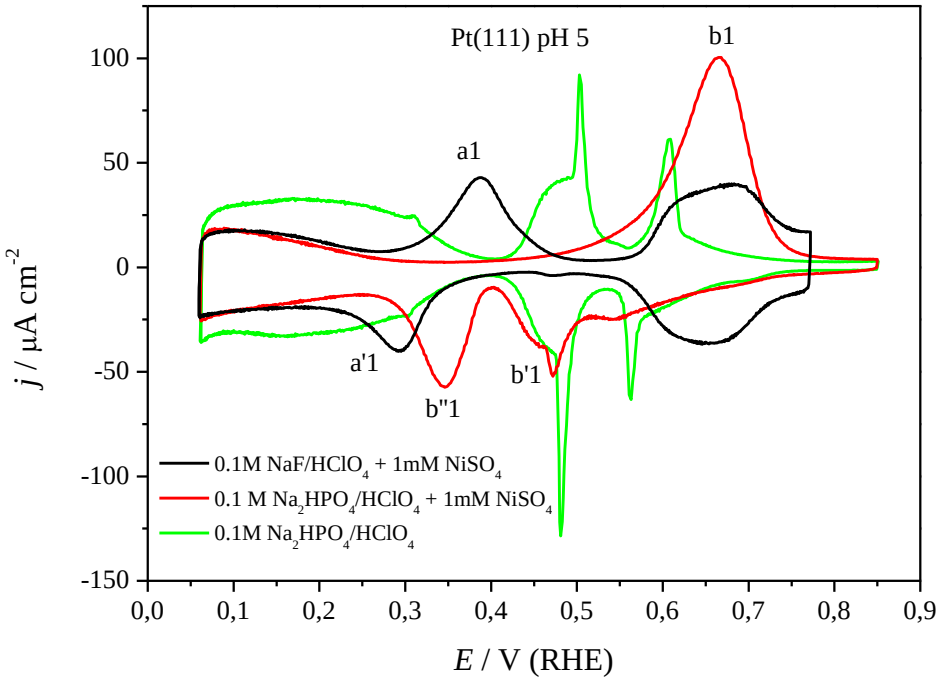

Figure 1. Cyclic voltammograms of the Pt(111) surface in 0.1M $NaF/HClO_4$ (pH 5) and 1mM $NiSO_4$ $6H_2O$ (Black), in 0.1M $Na_2HPO_4/HClO_4$ (pH=5) and 1mM $NiSO_4$ $6H_2O$ (red), and Pt(111) in 0.1M $Na_2HPO_4/HClO_4$ (pH=5) (green). Scan rate 50mV/s.

Figure 2 shows the cyclic voltammograms at pH 5 and 2mM $NiSO_4$ for different Na_2HPO_4 concentrations. When the concentration of phosphate increases, the peak corresponding to nickel oxidation appearing at 0.28 V (red curve) is shifted toward higher potentials (green curve) and is overlapped with the phosphate adsorption processes (blue and cyan curves). This reflects the synergic effect in which nickel shifts the pzfc toward lower potentials making possible the adsorption of phosphate at lower potentials, while phosphate ions increase the interaction Ni-Pt as it has been explained above.

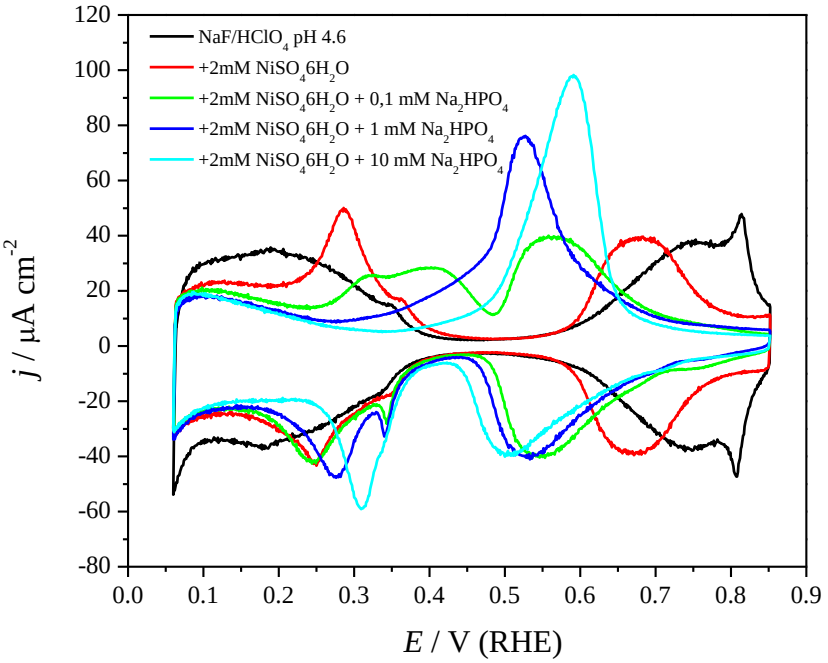

Figure 2. Cyclic voltammograms of the Pt(111) surface in $NaF/HClO_4$ (pH=4.6) (Black) and containing 2mM $NiSO_4\ 6H_2O$ with different concentrations of Na_2HPO_4. Without Na_2HPO_4 (red), and with 0.1, 1 and 10 mM Na_2HPO_4 (green, blue and cyan respectively). Scan rate 50mV/s.

3.2 Spectroscopic Analysis by FTIR

To obtain more information about this coadsorption process, the interphase was investigated using infrared spectroscopy. Figure 3 shows FTIR spectra collected for a Pt(111) surface in 0.2 M Na_2HPO_4 (pH=5) with and without nickel in solution. Both spectra show positive bands for adsorbed phosphate ions around 1150 cm^{-1}. The reference spectrum was collected at a low potential value, with the idea of eliminating the contributions from adsorbed phosphate at the reference spectrum. At this pH, $H_2PO_4^-$ ion is the predominantly phosphate species in the bulk solution. Therefore, we might tentatively ascribe the positive bands to the $H_2PO_4^-$ adsorbed species. However, it has been observed that for phosphate, bisulfate and other systems, Au and Pt surfaces can favor proton dissociation because of the electron donation from the adsorbed anion to the metal surface [13]. For example, on the Au(111) electrode at pH 5, HPO_4^{2-} is

preferentially adsorbed from the dihydrogen phosphate dominant solution [13a]. In addition, it has been reported by Weber et al. that $H_2PO_4^-$ undergoes a proton dissociation resulting to the adsorbed HPO_4^{2-} specie on Pt(111) at pH 2.8, when the potential is increased above 0.6 V vs Pd/H_2 [14]. In this work, on the Pt(111) surface without nickel (Figure 3A), a strong positive-going band is observed in the 1118-1165 cm^{-1} range above 0.4 V. This band can be ascribed to the symmetric A_1 stretching ($\delta(OH)+\nu_s(P\text{-}O_3^*)$) from the adsorbed HPO_4^{2-} via three oxygen atoms [15]. On the other hand, below 0.5V there is a positive band close to 1150 cm^{-1} corresponding to the antisymmetric $P\text{-}(OH)_2$ stretching vibrations of the $H_2PO_4^-$ ions in the bulk solution which is overlapped with the band of adsorbed species [14]. This species can be formed in the thin film due to acidification of the pH after the hydrogen desorption. When the solution contains nickel (Figure 3B) the positive going-band in the 1118-1168 cm^{-1} range appears already at 0.189 V. This fact agrees with the voltammetric trends discussed above, that suggest coadsorption of phosphate with the Ni^{2+} adsorbed on the Pt(111) surface at potentials below 0.35 V at pH~5. As mentioned above, nickel hydroxide adsorbed on Pt(111) surface causes a decrease of the electric field because of a shift of the potential of zero free charge (pzfc) to lower values [5a, 5c]. This results on a significant shift in the onset of phosphate adsorption to values lower than 0.189 V. At potentials above 0.2 V, a negative-going band is observed at 1106 cm^{-1}, and its intensity remains constant above 0.4 V, despite of the growth of the positive-going band at 1118 cm^{-1}. The negative band would correspond to phosphate adsorbed already at the reference potential. The positive shift of the band with the increase of the potential could be due to stark effect, or might indicate a change in the coordination geometry of the adsorbed anion [16]. The former would be related to the increase of the positive electric field as the applied potential is far from the pzc until the nickel oxidation at ~0.5 V (Figure 1). On the other hand, the nickel oxidation causes the desorption of the HPO_4^- ions from the nickel adlayer and the consequent adsorption on the Pt(111) surface, leading to a significant change in the coordination geometry of the adsorbed state above ~0.5 V. In both cases, for Pt(111) with and without nickel containing solution, negative bands around 1100 and 1064 cm^{-1} corresponds to vibrations of $H_2PO_4^-$ ions in solution [14].

10.1002/cphc.201900543

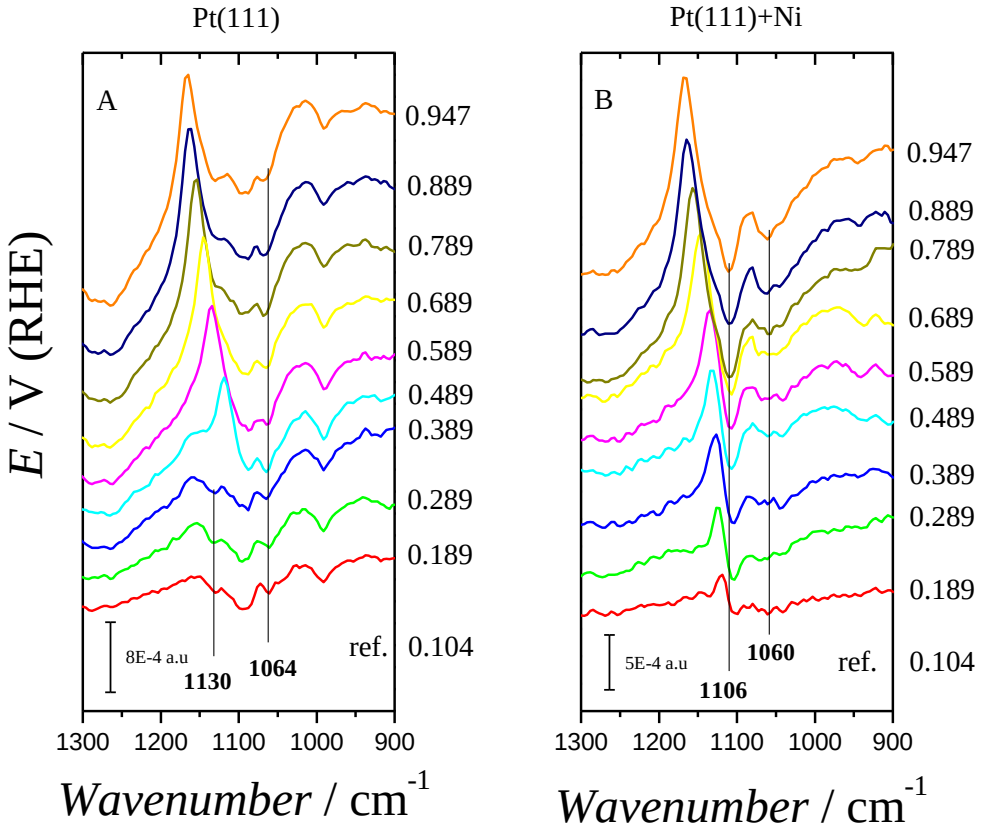

Figure 3. FTIR spectra taken with p-polarized light for the adsorbed phosphate ions on the Pt(111) surface, A) in 0.1M NaF, 0.2M Na_2HPO_4, 0.2M $HClO_4$ (pH=5); B) the same conditions with 1mM $NiSO_4$ $6H_2O$. The reference potential in both cases is 0.1 V. 200 interferograms were collected at each potential.

Additional information is obtained from the plot of the main band wavenumber for adsorbed phosphate as a function of the potential (RHE), as shown in figure 4. For the result without nickel, a straight line with single slope is obtained with an average value of 99 cm^{-1} V^{-1}. But, when the solution contains nickel, the line splits in two segments with a slope of 39 cm^{-1} V^{-1} when the surface is covered with nickel, in the low potential region, that joins the 99 cm^{-1} V^{-1} slope when nickel is oxidized. The change of slope coincides with the nickel oxidation peak, as the insert shows. This fact demonstrates that HPO_4^- is adsorbed on the nickel adlayer in the low potential region, but as the potential is scanned positively, nickel adatoms are stripped from the surface and the HPO_4^- ions are transferred to the underlaying platinum atoms. The larger shift of the

band center at Pt(111) than at Pt(111)-Ni_{ads} might be an indication of a stronger ion-metal interaction between phosphate and the bare Pt(111) substrate (stronger backdonation).

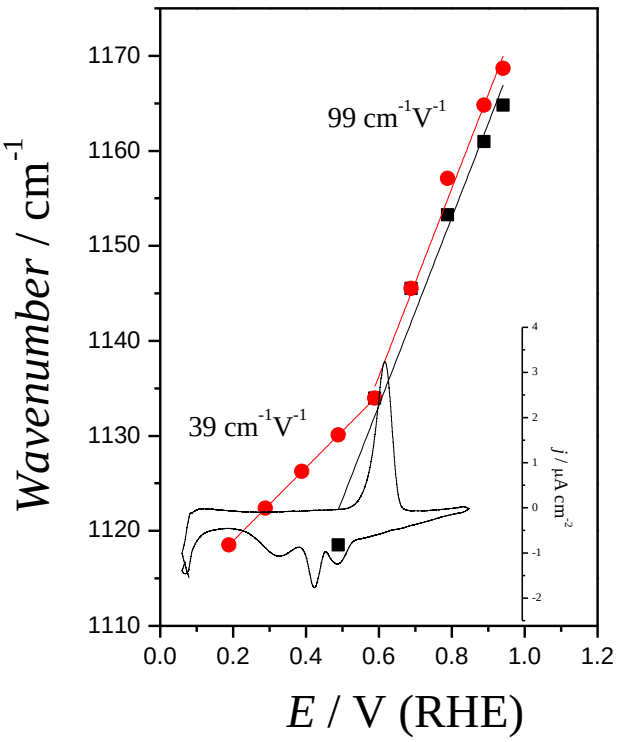

Figure 4. Plot of the wavenumber of the high-frequency mode corresponding to specie adsorbed on Pt (111) without nickel (black) and containing nickel in the solution (red) versus the potential (RHE) at pH=5. The insert shows the cyclic voltammogram for Pt(111) in 1mM $NiSO_4$ $6H_2O$ plus 0.1M $Na_2HPO_4/HClO_4$ recorded at 1mV/s for to approximate the scan rate to the one obtained in the IR experiment.

3.3 CO Displacement Measurements and Coulometric Analysis

The spectroscopic and voltammetric results discussed above suggest the existence of coadsorption phenomena between nickel and phosphate, shifting the onset of adsorption of phosphate to significantly low potential values. We have previously investigated the coadsorption of hydroxyl species on nickel adlayers on platinum in acid and alkaline solution using the CO charge displacement technique. In this case, CO was proved able

to adsorb on the nickel adlayer, displacing the hydroxyl adlayer [5b]. From the displaced charges, it is possible to obtain quantitative information about the amount of coadsorbed phosphate with nickel.

Figure 5A shows the transient currents obtained at 0.1V during charge displacements with CO for different concentrations of nickel and phosphate. In the case of 0.1M phosphate with no nickel in solution, a positive transient current is obtained corresponding to the displacement of the adsorbed hydrogen with a charge of 135μC/cm^2, in accordance with previous reports [17]. When there is nickel in solution but no phosphate, a transient current appears with both positive and negative contributions. As it has been reported, those contributions correspond to the remaining hydrogen adsorbed on the Pt(111) surface after nickel deposition and to the hydroxyl ions adsorbed on the nickel adlayer, respectively [5b]. Under the same conditions, but after adding a small amount of phosphate ions (0.1mM and 1mM) to solution, we tentatively might expect to obtain a higher negative contribution due to the displacement of coadsorbed phosphate, according to the results previously discussed. However, for small phosphate concentration, the resulting net charge (addition of the positive and negative contributions) is nearly the same (-58.4, -61.3 and -63 μC/cm^2 for 0, 0.1 and 1 mM phosphate concentration, respectively). In the three cases, the time in which the working electrode was kept at 0.1 V was the same (21s), to avoid that variations in this parameter could affect the amount of deposited nickel. Increasing this time to 180 s, for 1mM phosphate ions, the registered net charge remains unchanged (-63 μC/cm^2). However, for the same time at 0.1V (180s) but increasing the Na_2HPO_4 concentration to 0.1 M, only a small positive transient current is obtained (5.2 μC/cm^2) corresponding to some small amount of remaining hydrogen adsorbed on the Pt(111) surface. This result can be explained considering that phosphate binds on the nickel adlayer stronger than OH and cannot be displaced by CO. Those results are in accordance with their respective CO stripping profiles shown in figure 5B (full line). This figure shows the CO stripping curves corresponding to each CO displacement (full line) and the same without CO (dash dot). As it can be seen in this figure, for 1mM $NiSO_4$ without phosphate, two peaks are recorded on the positive-going scan at 0.37 and 0.75 V associated to the nickel oxidation and CO oxidation respectively. Details of this process have been given previously [18]. With 0.1mM and 1mM Na_2HPO_4 with nickel in the solution, keeping the working electrode 21s at 0.1V, the same peaks are observed

but the first one is shifted 40mV toward lower potentials. This could be the result of phosphate causing a less compact nickel adlayer on the Pt(111) surface. Although phosphate seems to stabilize the nickel on the surface in this experiment the amount of phosphate is very small and has been displaced with CO (as concluded from the CO displacing transient). The second peak at 0.75 V is nearly the same with and without phosphate. For the experiment involving 0.1M phosphate plus 1mM nickel sulphate, only one peak is observed at 0.7V in the positive going scan during the CO stripping (figure 5B, curve i). This is similar to the one observed in the analogous voltammogram without CO (figure 5B, curve j). This confirms that only a small amount of CO was adsorbed in this case. The intermediate case (1mM Na_2HPO_4 and 180s at 0.1V) is explained below.

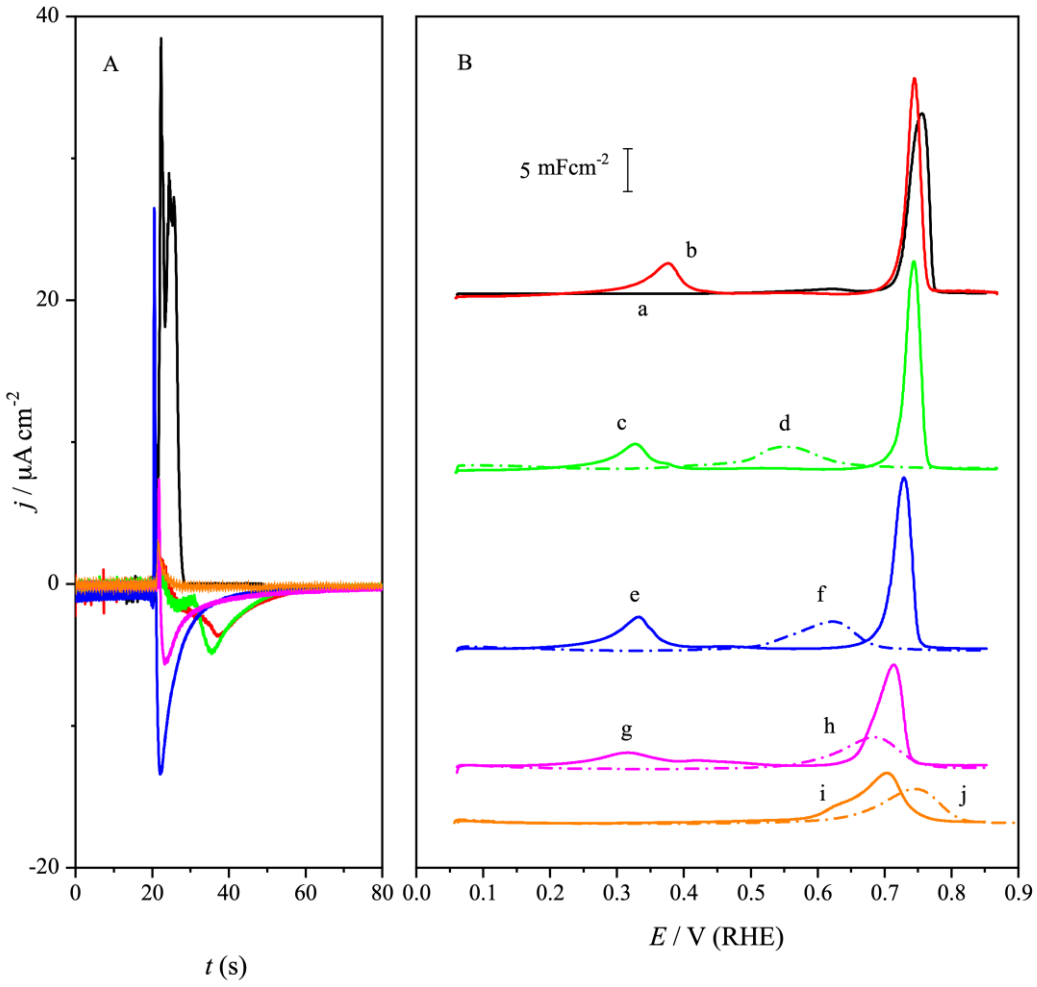

Figure 5. A) Transient current registered versus time at 0.1 V during CO charge displacement for different concentrations of nickel sulphate and disodium monohydrogenphosphate at pH 5. The time in which the working electrode was kept at 0.1 V was controlled since this affects the amount of deposited nickel. B) Plot of j/v corresponding to CO stripping for each charge displacement experiment in panel A) respectively, recorded at 20mV/s (full line) and the same without CO displacement, recorded at 50mV/s (dash dot). 0.1M Na_2HPO_4 line a (black); 0.1M NaF/$HClO_4$ + 1mM $NiSO_4$ and 20 s at 0.1V line b (red); 0.1M NaF/$HClO_4$ + 0.1mM Na_2HPO_4 + 1mM $NiSO_4$ and 20 s at 0.1V with and without CO lines c and d (green; full line and dash dot line respectively); 0.1M NaF/$HClO_4$ + 1mM Na_2HPO_4 + 1mM $NiSO_4$ and 20 s at 0.1V with and without CO lines e and f (blue; full line and dash dot line respectively); 0.1M NaF/$HClO_4$ + 1mM Na_2HPO_4 + 1mM $NiSO_4$ and 180 s at 0.1V with and without CO lines g and h (magenta; full line and dash dot line respectively); 0.1M NaF/$HClO_4$ + 1mM Na_2HPO_4 + 0.1M $NiSO_4$ and 180 s at 0.1V with and without CO lines i and j (orange; full line and dash dot line respectively).

From the analysis of the integrated charge involved in the different peaks for CO stripping, it is possible to obtain additional information about the amount of deposited nickel. The nickel oxidation peak at ca. 0.39 V in the solution without phosphate gives a charge of 173μC/cm^2. This charge remains very similar when small amounts of phosphate are added to the solution (157μC/cm^2 and 178 μC/cm^2 are obtained for 0.1mM Na_2HPO_4 and 1mM Na_2HPO_4 solutions, respectively). These charge values can also be compared with the result obtained without CO. For this, we use the voltammograms obtained after holding the electrode potential at 0.1V during 21 s (dashed lines in figure 5B, 187 and 215 μC/cm^2 for 0.1 and 1mM Na_2HPO_4 , respectively). However, the charge comparison is not straightforward, since the amount of coadsorbed anions may change significantly after the introduction of CO if CO is able to displace a fraction of the coadsorbed phosphate. At this point, it is puzzling how the introduction of CO in this case favors the oxidation of nickel, displacing it to significantly lower potentials, while the result with higher phosphate concentration suggests that CO is not able to displace phosphate on nickel. To reconciliate those results we suggest that the ability of CO to displace the adsorbed phosphate depends on the bulk phosphate concentration or the phosphate amount at the interface (explained

below). Then, for small phosphate concentration, CO is able to displace the coadsorbed phosphate. Without coadsorbed phosphate, the CO covered nickel adlayer behaves similarly to the one obtained when there is no phosphate in solution. In fact, the involved charges in the first peak of the stripping are very similar for 1mM $NiSO_4$ without phosphate and with 0.1 and 1mM Na_2HPO_4. In addition, the second peak in the stripping (at ca. 0.75 V) shows also similar charges (359, 374 and 374 μC/cm^2 without phosphate and with 0.1 and 1mM Na_2HPO_4 respectively). On the other hand, when phosphate concentration increases to 0.1M, the formation of a more compact adlayer precludes the CO displacement and the stripping sweep is very similar to the result without CO in the adlayer. This is shown in figure 5B (orange full line/ dash dotted line, curves i and j, respectively). In this case, the charge involved under the stripping peak (293 μC/cm^2) is closer to the one observed in the analogous voltammogram without CO (244 μC/cm^2). All these charge values are collected in table 1.

μC/cm^2	q^1_{strip}	q^2_{strip}	q without CO
0.1M Na_2PO_4	-	418	113
1mM $NiSO_4$+0.1M NaF/$HClO_4$	173.3	359	-
+0.1mM Na_2HPO_4 (21s at 0.1V)	157	374	187
+1mM Na_2HPO_4 (21s at 0.1V)	178	374	215
+1mM Na_2HPO_4 (180s at 0.1V)	122	302	224
+0.1M Na_2HPO_4 (180s at 0.1V)	-	293	244

Table 1. Charge of stripping with CO and without CO shown in figure 5.

An intermediate nickel coverage between the extreme situations described above is obtained by holding the potential at 0.1 V during a longer time, 180 s, in the 1mM $NiSO_4$ plus 1 mM Na_2HPO_4 solution. In this case, the charge of the first and the second stripping peaks (122 μC/cm^2 and 302 μC/cm^2) are smaller than the corresponding

values for 0.1 and 1mM Na_2HPO_4, 21 s. By increasing the polarization time at 0.1V, the nickel amount adsorbed on the electrode surface increases [5b]. Therefore, these results can be rationalized by considering that, when the nickel coverage increases, the phosphate adsorption is induced in higher degree, making more difficult the displacement by CO. Therefore, the ability of CO to displace the adsorbed phosphate depends on the amount of phosphate adsorbed at the interface.

To obtain more information on the role of the electrode potential on the ability to displace coadsorbed phosphate, the CO displacement experiment was repeated at higher potentials. Figure 6 shows the transient currents obtained during the CO displacement at 0.3 V (as before, the electrode potential was kept 21s at this potential before the experiment) for 1mM $NiSO_4$ plus 1mM and 0.1M Na_2HPO_4. In this case, only a positive current is obtained with an involved charge of 100 μC/cm^2 for both phosphate concentrations. This situation suggests two possibilities. One possibility would be that CO displaces both Ni and phosphate, with the result of a net positive charge.

$$Pt - Ni(HPO_4)_n + CO \longrightarrow Pt - CO + Ni^{2+} + nHPO_4{}^{2-} + (2-2n)e \quad (1)$$

where we have considered, according to the spectroscopic data that the adsorbed species is HPO_4^{2-}. On the other hand, a second possibility would be that only the phosphate anion is displaced by CO, resulting in a CO covered nickel adlayer. This would be similar to the result previously observed at 0.1 V in the absence of phosphate.

$$Pt - Ni(HPO_4)_n + CO + 2ne \longrightarrow Pt - NiCO + nHPO_4{}^{2-} \quad (2)$$

After the removal of the phosphate the Ni would be destabilized and finally oxidized

$$Pt - NiCO \longrightarrow Pt - CO + Ni^{2+} + 2e \quad (3)$$

Addition of equations (2) and (3) results again in equation (1). In those equations, *n* is the number of HPO_4^{2-} species per nickel adatom. Considering that displaced charge is positive, the only possible value for *n* is n<1 (higher values of *n* would result in negative displaced charges).

The resulting stripping sweep after the CO displacement at 0.3 V only shows a peak in the positive-going scan with a charge of 414 and 420 μC/cm^2 for 1mM and 0.1M Na_2HPO_4 respectively (figure 6B). These charges are the same as the one obtained for 0,1M Na_2HPO_4 without nickel in the solution (shown in figure 5B and table 1). This

result reflects that the whole nickel adlayer is removed from the surface electrode during the displacement with CO. Therefore, it is possible to describe the obtained charge during the displacement with the following equation:

$$q_{net}^{d} = (2 - 2n)\, q_{111}\theta_{Ni} \quad (4)$$

where q_{net}^{d} is the displaced net charge and q_{111} is the charge corresponding to one electron per Pt atom on the (111) surface (240 μC/cm^2). The nickel coverage in the absence of phosphate can be obtained from the displaced charge using the equation 5 previously reported [5b].

$$\theta_{Ni} = \frac{q_{H,0.1}^{\theta=0} - q_{net}^{d}}{2\, q_{111}} \quad (5)$$

where $q_{H,0.1}^{\theta=0}$ is the hydrogen charge on the blank experiment recorded at 0.1 V in the absence of nickel (136.5 μC/cm^2). Using equation 5 for the result corresponding to a polarization time of 20s (q_{net}^{d} = -58.4, see above), the obtained nickel coverage (θ_{Ni}) is ca. 0.4. Introducing this value in the equation 4 (assuming that the nickel coverage is similar in the presence of phosphate) it is possible to give an estimation of the number of HPO_4^{2-} adsorbed for each nickel adatom, resulting a value of *n* close to 0.5.

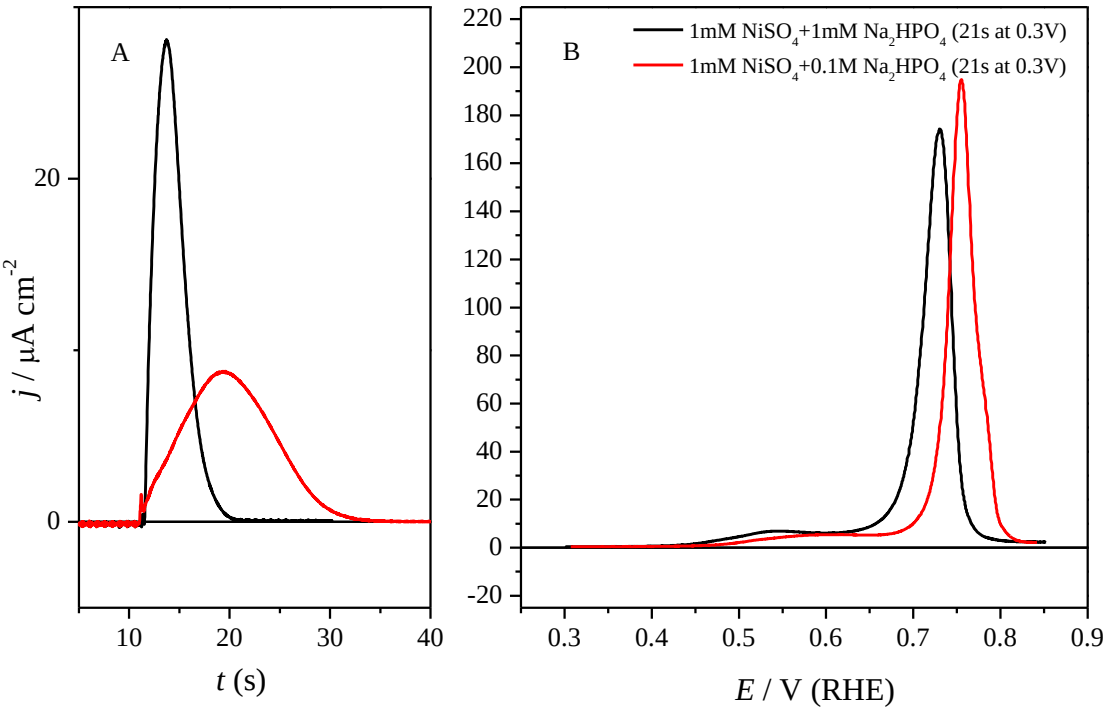

Figure 6. A) Transient current registered versus time at 0.3 V during CO charge displacement technique for different concentration of disodium monohydrogenphosphate at pH 5. The time in which the working electrode was kept at 0.3 V (21s) was controlled because it affects the amount of deposited nickel. B) CO stripping after each charge displacement experiment respectively, recorded at 20mV/s.

3.4 Laser-Induced Temperature Jump Technique

The CO displacement technique provides information about the nature of adsorbed species, allowing the distinction between adsorbed cations and anions. However, it does not give any indication about the nature of the electric field on the surface that could give clues to explain why the anion is adsorbed at lower potentials when nickel is in solution. On this subject, the laser temperature jump technique provides information related with the magnitude and sign of the electric field at the interphase. In this technique, the temperature of the interfacial region is increased using pulsed laser irradiation, causing a disorder of the network solvent molecules at the interface. This originates a change in the electrode potential which is recorded under coulostatic

conditions. The potential transient shows the magnitude and sign of the electric field on the electrode surface and is closely linked with the orientation (dipolar contribution) of the solvent molecules on the surface electrode [11a, 11b, 19]. Therefore, at potentials below the pzfc, where the surface has negative charge, solvent molecules are oriented with the atoms with partial positive charge pointing to the surface, originating in this way a positive dipolar contribution and negative transient ΔE vs t is recorded. Conversely, when the applied potential is above the pzfc, the dipolar contribution is negative and a positive laser induced transient is obtained. Close to the pzfc, transients are nearly zero because there is not net dipolar contribution. In this point, the interfacial solvent network reaches the maximum disorder and this potential value corresponds to the potential of maximum entropy of double layer formation (pme).

Figure 7 shows the laser induced potential transients obtained for Pt(111) at 0.16V in 0.1M NaF/$HClO_4$ (pH 5) without and with nickel using different concentrations of Na_2HPO_4. As can be seen, the transient for Pt(111) in 0.1M NaF/$HClO_4$ without nickel (Black) is negative. This means that the interfacial water molecules orientate with their hydrogen atoms pointing toward the electrode surface. When nickel is added into the solution, the pzfc shifts toward negative potentials and the transient is inverted because of a change in orientation of the solvent dipoles. Finally, when phosphate is added in addition to nickel, the transients turn negative again. Those transients are more negative as the Na_2HPO_4 concentration increases. However, we would have expected the opposite, that is, if phosphate stabilizes the deposited nickel, the potential transient would be more positive. The only way to explain the observed trend is to consider that coadsorbed phosphate in the IHP is causing a screening of the positive electric field on the electrode surface or that there is even a superequivalent phosphate adsorption resulting in an inversion of the electric field at the OHP. Such inversion has already been observed for sulfate and during the oxidation of the platinum surface at high potentials.

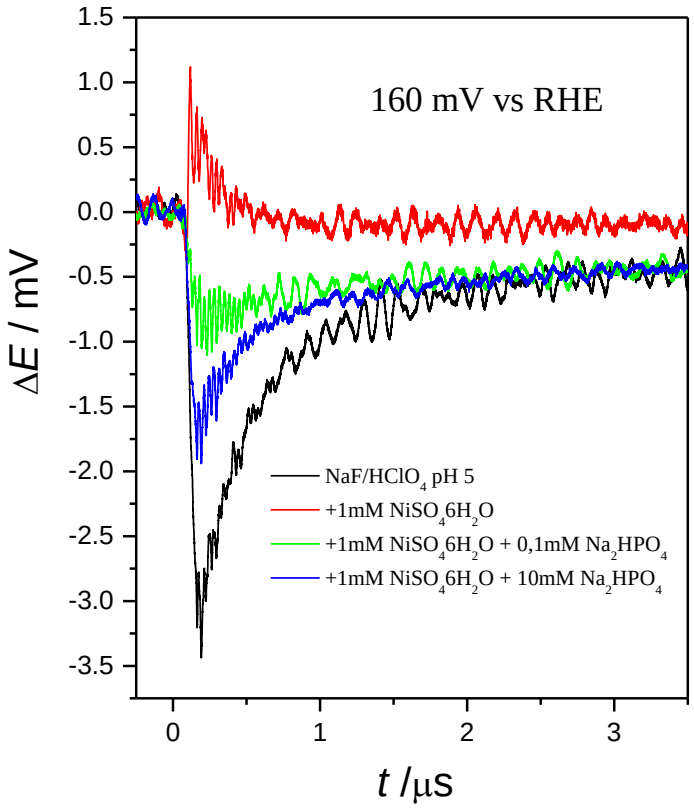

Figure 7. Laser transients at 160 mV vs RHE for 0.1 M $NaF/HClO_4$ (pH=5) (Black) and containing 1mM $NiSO_4$ $6H_2O$ with different concentrations of Na_2HPO_4. Without Na_2HPO_4 (red), and with 0.1 and 10 mM Na_2HPO_4 (green and blue respectively). In all cases the working electrode was kept during 4.5 min at 0.16 V prior to registering the laser potential transients, to obtain the same nickel amount adsorbed on the surface electrode.

3.5 Voltammetric Characterization of HER

We turn now to the study of the effect of nickel and phosphate on the rate of HER. Before this, it is convenient to study the process of bulk deposit of nickel. In this way, it is possible to infer if the current density obtained during the HER contains a significant

contribution from nickel reduction. We selected for this a glassy carbon electrode because on this surface the rate of HER is very small. Figure 8A shows the negative-going scan to sufficiently negative potentials on a glassy carbon electrode for different concentrations of nickel, obtained with a rotating disk electrode (2500 rpm) to control the rate of mass transport. For each nickel concentration, a stable current is only reached in the second or third cycle after the first excursion to sufficiently negatives potentials where the nickel deposit is originated. In the particular experiment for 0.5 mM $NiSO_4$ shown in figure 8A, the first cycle was reversed before reaching a sufficiently high current. In this case, the stable voltammogram was attained in the third cycle. On the other hand, for the experiments containing 0.1mM and 1mM nickel sulphate, where a sufficiently high current was attained in the first cycle, the second cycle is already stable. These results can be explained considering that the first cycle represents the initial nickel deposition in the bare glassy carbon while the stable voltammogram gives a measure of the nickel catalyzed HER current. Assuming that bulk deposition of nickel starts at nearly the same potential on Pt and on glassy carbon, these results can help us to understand the results shown for Pt(111) in figure 8B. With this information we can propose that the first wave between 0 and -0.25 V corresponds to hydrogen production through proton reduction. This reaction is limited by the mass transport of protons or the protonated form of the buffer. The bulk nickel deposition for 1mM $NiSO_4$ would start at ca. -0.35V according to the result for glassy carbon. From this potential, the nickel deposit competes with the water splitting on the surface of the electrode. As more cycles are registered, the negative current increases because of an increase in the catalytic activity towards the HER caused by the accumulation of nickel on the surface. On the other hand, the corresponding peak of nickel oxidation centered at 0.23V decreases. After several cycles, the voltammogram reaches a stationary state with an enhanced catalytic activity for the HER.

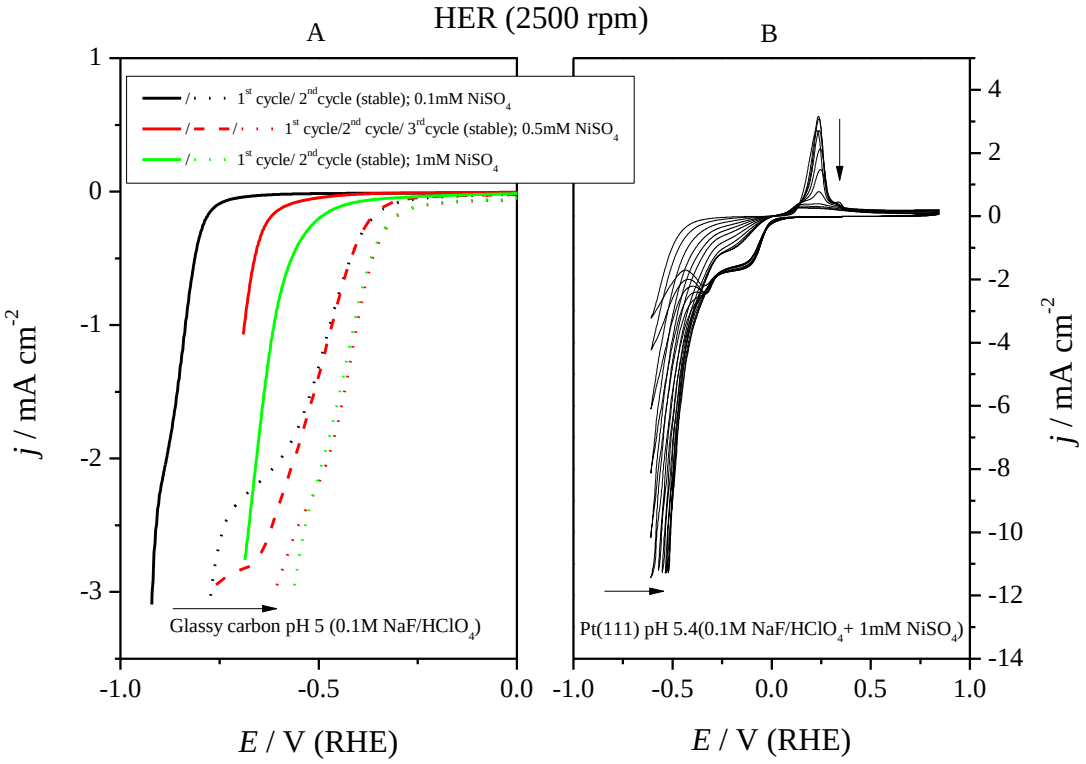

Figure 8. A) HER on glassy carbon electrode at pH 5 (0.1M NaF/$HClO_4$) for different concentrations of $NiSO_4$: 0.1mM (Black), 0.5mM (Red) and 1mM (Green). B) HER on Pt(111) at pH ~5 (0.1M NaF/$HClO_4$) for 1mM $NiSO_4$. The ohmic resistance was corrected. Scan rate 50mV/s; 2500 rpm.

Figure 9 shows the hydrogen evolution reaction (HER) at pH 5 for Pt (111) with and without nickel in solution, and the effect of the presence of phosphates with nickel. When nickel is in solution, the water splitting is shifted approximately 160 mV towards more positive potentials. On the other hand, the rate of the first wave corresponding to HER from the proton reduction is not affected by the presence of nickel. When phosphate is added, the onset of this initial wave is shifted ca 40mV towards more negative potentials, while the limiting current significantly increases. As mentioned above, this initial wave most likely correspond to hydrogen formation from proton reduction. In the presence of a buffer system, the protonated form of the acid base couple is responsible for supporting the transport of protons. At pH 5 the amount of protonated buffer species in equilibrium in the bulk solution under present conditions are 0.0017M HF and 0.01M $H_2PO_4^-$. Therefore, to account for this difference, figure 10

shows the current densities divided by the limiting current density in the first plateau for HER.

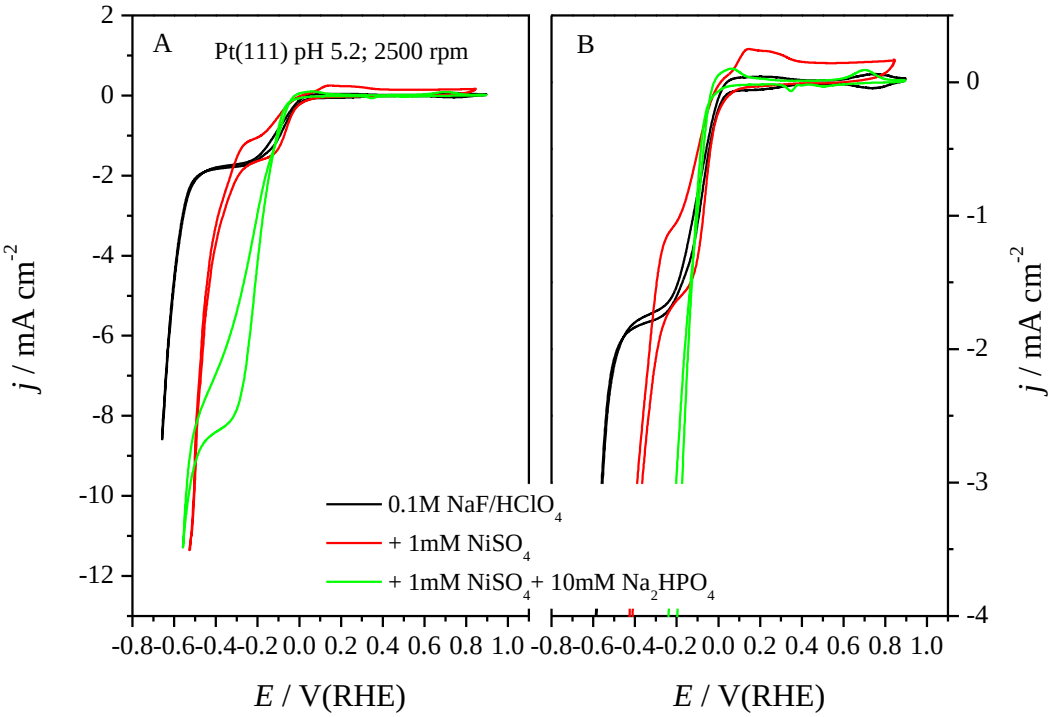

Figure 9. A) HER for Pt(111) surface in 0.1M $NaF/HClO_4$ (pH 5) (Black); 0.1M $NaF/HClO_4$ (pH 5) plus 1mM $NiSO_4$ $6H_2O$ (red); 0.1M $NaF/HClO_4$ (pH 5) plus 10mM Na_2HPO_4 and 1mM $NiSO_4$ $6H_2O$ (green). B) Enlargement of the voltammetric current from -4 to 0.5 mA/cm^{-2}. The ohmic resistance was corrected. Scan rate 50mV/s; 2500 rpm.

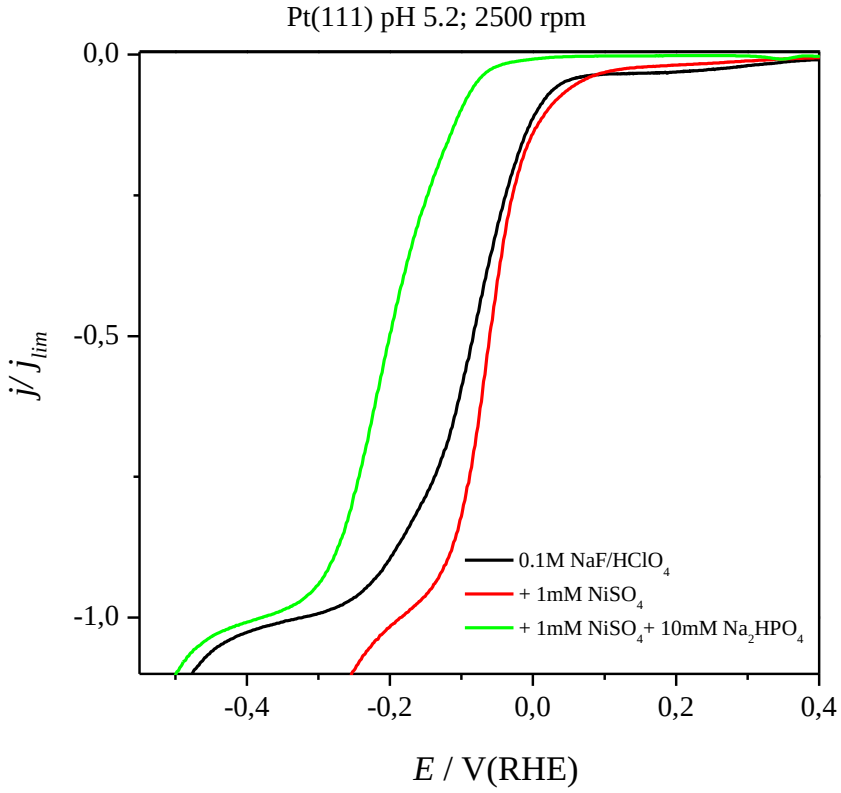

Figure 10. Current density of HER divided by the limiting current density in the first plateau in 0.1M $NaF/HClO_4$ (pH 5) (Black), 0.1M $NaF/HClO_4$ (pH 5) plus 1mM $NiSO_4$ $6H_2O$ (red) and 0.1M $NaF/HClO_4$ (pH 5) plus 10mM Na_2HPO_4 and 1mM $NiSO_4$ $6H_2O$ (green). Scan rate 50mV/s; 2500 rpm.

This comparison clearly evidences that the presence of phosphate hinders the HER. One possibility to explain this result is to consider that the co-adsorbed phosphate ions on the surface electrode hampers the diffusion of the proton through the double layer. This adsorption is induced by a shift of the potential zero charge (pzc) caused by the adsorbed nickel on the surface. It has been previously proposed that the benefit from nickel modification of the platinum surface is related with the shift of the pzfc and its effect to water transport through the interphase. This conclusion was supported by the laser induced temperature jump experiment that demonstrated a significant decrease of the electric field after nickel modification. In the present paper, we have demonstrated that the addition of phosphate leads to anion coadsorption that results in a neutralization of this effect. It is important to remark that the current of HER for 1mM $NiSO_4$ without phosphate in figures 9 and 10 corresponds to the last cycle (stable cycle). However,

when phosphate is in solution the cycles for the HER are stable from the beginning. This fact shows that the adsorbed phosphate stabilizes the nickel adlayer.

4. Conclusion

The cyclic voltammograms obtained for different phosphate concentrations show the existence of a coadsorption phenomenon between nickel and phosphate ions. This is corroborated using the infrared spectroscopy technique (FTIRRAS), where, in the presence of nickel, adsorbed phosphate species can be observed at very low potentials (< 0.2) compared to the same experiment without nickel in solution. This technique reveals the adsorption of the HPO_4^{2-} species on the electrode surface from the $H_2PO_4^-$ ions present in the bulk solution. When nickel is adsorbed on the electrode surface, the adsorbed HPO_4^{2-} ions undergo a change in the adsorption geometry. This can be caused by the change of the electric field on the surface when moving towards positive potentials or by the desorption of the nickel adlayer that allows the entrance of phosphate ions on the platinum surface. The CO charge displacement technique confirms the existence of a synergic effect between co-adsorbed nickel and phosphate resulting in an extra stabilization of the adlayer. In this regard, at high phosphate concentration CO is unable to displace the coadsorbed anions from the adlayer. At higher potentials, CO is able to displace both nickel and the adsorbed anions. A displacement of the pzc towards negative potentials after nickel deposition might be the reason for the extra stability of the mixed nickel phosphate adlayer. In this way, a more positive surface is obtained after nickel deposition that facilitates phosphate adsorption. This trend is also corroborated by the laser temperature jump technique.

The previous conclusions are used to rationalize the effect of nickel and phosphate on the rate of HER. The presence of nickel enhances the rate of HER, in agreement with previous reports, where it was observed that nickel displaces the pzc/ pme towards values close to the equilibrium potential of the hydrogen reduction reaction. This increases the disorder in the interfacial solvent network, facilitating the diffusion of protons through the double layer, improving the hydrogen evolution reaction [5a, 5c]. In the presence of phosphate, the anions adsorbed on the nickel adlayer hampers the access of protons to the surface and therefore hinders the hydrogen evolution reaction.

Acknowledgments

This work has been financially supported by the MINECO (Spain) project No. CTQ2016-76221-P.

References

[1] T. Bligaard, J. K. Norskov, *Electrochim. Acta* **2007**, *52*, 5512-5516.
[2] a)V. R. Stamenkovic, B. Fowler, B. S. Mun, G. F. Wang, P. N. Ross, C. A. Lucas, N. M. Markovic, *Science* **2007**, *315*, 493-497; b)K. Wang, H. A. Gasteiger, N. M. Markovic, P. N. Ross, *Electrochim. Acta* **1996**, *41*, 2587-2593.
[3] a)E. Leiva, T. Iwasita, E. Herrero, J. M. Feliu, *Langmuir* **1997**, *13*, 6287-6293; b)A. Cuesta, *ChemPhysChem* **2011**, *12*, 2375-2385.
[4] E. Herrero, L. J. Buller, H. D. Abruna, *Chemical Reviews (Washington, DC, United States)* **2001**, *101*, 1897-1930.
[5] a)I. Ledezma-Yanez, W. D. Z. Wallace, P. Sebastián-Pascual, V. Climent, J. M. Feliu, M. T. M. Koper, *Nature Energy* **2017**, *2*, 17031-17037; b)F. J. Sarabia, V. Climent, J. M. Feliu, *J. Electroanal. Chem.* **2018**, *819*, 391-400; c)F. J. Sarabia, P. Sebastian-Pascual, M. Koper, V. Climent, J. M. Feliu, *ACS Applied Materials & Interfaces* **2018**, 10.1021/acsami.1028b15003.
[6] Z. Shi, S. Wu, J. Lipkowski, *Electrochim. Acta* **1995**, *40*, 9-15.
[7] a)B. E. Logan, B. Hamelers, R. Rozendal, U. Schroder, J. Keller, S. Freguia, P. Aelterman, W. Verstraete, K. Rabaey, *Environmental Science & Technology* **2006**, *40*, 5181-5192; b)L. Murphy, *Current opinion in chemical Biology* **2006**, *10*, 177-184.
[8] a)J. Clavilier, D. Armand, S. G. Sun, M. Petit, *J. Electroanal. Chem.* **1986**, *205*, 267-277; b)C. Korzeniewski, V. Climent, J. M. Feliu, in *Electroanalytical Chemistry: A Series of Advances, Vol. 24* (Eds.: A. J. Bard, C. Zoski), CRC Press, Boca Raton, **2012**, pp. 75-169.
[9] V. Climent, R. Gómez, J. M. Feliu, *Electrochim. Acta* **1999**, *45*, 629-637.
[10] a)F. C. Nart, T. Iwasita, *Electrochim. Acta* **1992**, *37*, 385; b)F. C. Nart, T. Iwasita, M. Weber, *Berichte der Bunsen-Gesellschaft fuer Physikalische Chemie* **1993**, *97*, 737.
[11] a)V. Climent, B. A. Coles, R. G. Compton, *J. Phys. Chem. B* **2002**, *106*, 5988-5996; b)V. Climent, B. A. Coles, R. G. Compton, *J. Phys. Chem. B* **2002**, *106*, 5258-5265; c)N. Garcia-Araez, V. Climent, J. M. Feliu, *J. Am. Chem. Soc.* **2008**, *130*, 3824-3833.
[12] a)R. Martínez-Hincapié, P. Sebastián-Pascual, V. Climent, J. M. Feliu, *Electrochem. Commun.* **2015**, *58*, 62-64; b)R. Rizo, E. Sitta, E. Herrero, V. Climent, J. M. Feliu, *Electrochim. Acta* **2015**, *162*, 138-145.
[13] a)M. Yaguchi, T. Uchida, K. Motobayashi, M. Osawa, *J. Phys. Chem. Lett.* **2016**, *7*, 3097-3102; b)Z. F. Su, V. Climent, J. Leitch, V. Zamlynny, J. M. Feliu, J. Lipkowski, *Phys. Chem. Chem. Phys.* **2010**, *12*, 15231-15239; c)N. Garcia-Araez, V. Climent, P. Rodriguez, J. M. Feliu, *Langmuir* **2010**, *26*, 12408-12417; d)Z. Shi, J. Lipkowski, M. Gamboa, P. Zelenay, A. Wieckowski, *J. Electroanal. Chem.* **1994**, *366*, 317-326; e)R. Jinnouchi, T. Hatanaka, Y. Morimoto, M. Osawa, *Phys. Chem. Chem. Phys.* **2012**, *14*, 3208−3218.
[14] M. Weber, F. C. Nart, I. R. deMoraes, T. Iwasita, *J. Phys. Chem.* **1996**, *100*, 19933-19938.
[15] M. Weber, F. C. Nart, *Electrochim. Acta* **1996**, *41*, 653-659.
[16] K. Ataka, T. Yotsuyanagi, M. Osawa, *J. Phys. Chem.* **1996**, *100*, 10664-10672.

[17] a)V. Climent, R. Gómez, J. M. Orts, A. Aldaz, J. M. Feliu*, Vol. 97-17*, The Electrochemical Society, Inc., Pennington, NJ, **1997**, pp. 222-237; b)V. Climent, R. Gómez, J. M. Orts, A. Aldaz, J. M. Feliu*, Vol. 2000-16*, The Electrochemical Society, Inc., Pennington, NJ, **2000**, pp. 12-30.
[18] F. J. Sarabia, V. Climent, J. M. Feliu, *J. Electroanal. Chem.* **2017**, *819*, 391-400.
[19] V. Climent, N. Garcia-Araez, R. G. Compton, J. M. Feliu, *J. Phys. Chem. B* **2006**, *110*, 21092-21100.

10.1002/cphc.201900543

Table of Contents

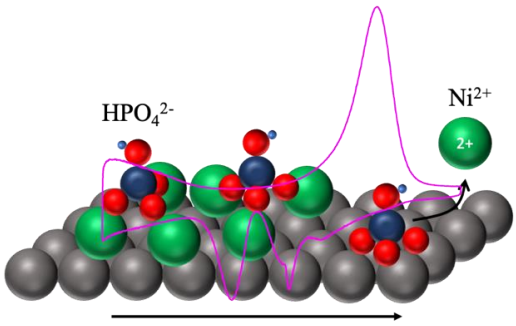

The presence of nickel deposits on Pt(111) induces phosphate adsorption at low potentials. This is due to a negative shift of the potential zero charge induced by nickel adsorption, creating a positive surface at lower potentials. Phosphate coadsorption stabilizes the nickel adlayer, that oxidizes at much higher potentials. The mixed nickel phosphate adlayer has been investigated using FTIRRAS, CO charge displacement and temperature jump. Hydrogen evolution in the presence of this adlayer is investigated using rotating disk electrode.